Applied Biological Research 27(2): 193-203; (2025)
DOI: 10.48165/abr.2025.27.01.19

DECIPHERING AIRBORNE MICROBIAL COMMUNITIES: LEVERAGING RNA APTAMERS VIA COMPUTATIONAL SLEUTHING

Rameshnath Raagavibai[1], Periyasamy Vijayalakshmi[1,2], Sounderraajan Aishwariya[1,2], Murugesan Viji[1,2], and Manikkam Rajalakshmi[1,2,3*]

[1]PG & Research Department of Biotechnology and Bioinformatics, [2]DBT-BIF Centre, [3]PG & Research Department of Zoology, Holy Cross College (Autonomous), Tiruchirappalli - 620 002 [Affiliated to Bharathidasan University], Tamil Nadu (India)
*****e-mail: *rajalakshmi@hcctrichy.ac.in*

(Received 25 December, 2024; accepted 3 June, 2025)

ABSTRACT

Airborne pathogens are a substantial threat to human health, hence an efficient mean to identify these contaminant is necessary to control their spread. The present work focused on developing the innovative concepts of employing RNA aptamers for the detection of biological pollutants in indoor air environment. The RNA aptamers are promising tool for detecting indoor air microbes, enhancing air quality and human health. This study utilized computational methods to identify and characterize RNA aptamer target interactions. The study used *in silico* techniques to design and predict aptamer sequence that can bind to various target microbial cells present in air. Based on computational validation we identified lead aptamer candidates by optimizing and refining aptamer sequence to demonstrate strong interactions with multiple microbial targets. RNA aptamer sequences were analysed to retrieve various properties using oligo-sequence analyzer. Secondary structures were predicted using RNA fold, followed by 3D structure prediction by RNA Composer and H-Dock server to perform RNA-protein docking. Interaction modalities were explored using PHLIP server. RNA aptamer 1, 2, and 3 showed strong binding affinity score of -344.95, -331.99 and -395.58 with target proteins. All aptamers showed robust hydrophobic and hydrogen bond interaction with their guanidine phosphate backbone mediated interactions with Val, Lys, Arg, and Asp amino acid residues of target proteins. The *in vitro* synthesis and *in situ* environmental validation will provide necessary way to implement this aptamer-protein interaction into real time monitoring places like healthcare, air quality assessment framework and environmental analysis.

Keywords: Airborne microbial communities, Indoor air quality, public health, RNA aptamers, computational modelling, molecular docking

INTRODUCTION

Infectious diseases are one of the primary impediments to human health. Controlling the spread of infectious diseases requires early and accurate detection of microorganisms. Airborne pathogens pose serious threat to public health, causing a wide range of respiratory illnesses and contributing to the spread of infectious diseases worldwide (Chawla *et al.*, 2023). The transmission of pathogens through indoor air lead to various respiratory illnesses. Factors like droplets from coughing or sneezing, inadequate ventilation systems, and overcrowding contribute to the proliferation of indoors microbes. Monitoring and surveilling microbial populations in indoor air are essential for safeguarding public health and mitigating the spread of infectious diseases. The presence of microbial pollutants in various indoor environments, emphasize the need for accurate detection methods (Acharya *et al.*, 2018).

The World Health Organization (WHO) has highlighted the urgency of addressing resurgence of airborne infectious diseases, particularly amidst COVID-19 pandemic (Morawska *et al.,* 2022). Indoor air pollution is a contributing factor to an exacerbation of 50% of all illnesses. In India, nearly 100,000 patients perish from hospital-acquired illnesses every year, accounting for 2 million cases. Nasobronchial allergies and aeroallergens affect about 5% of Indians and it has been discovered that indoor air contains up to 70 times more dangerous toxins than outdoor air (Annadurai *et al.,* 2024). Indoor air pollution predominantly arises from microbial pollutants originating from diverse sources, including human occupants, pets, outdoor air, and building materials. These microorganisms, pose significant health risks. Common pathogens frequently found indoors include *Staphylococcus aureus, Clostridium difficile, Acinetobacter baumannii, Pseudomonas aeruginosa, Mycobacterium tuberculosis, Streptococcus pneumonia, Legionella pneumophila, Aspergillus* spp., *Candida* spp., mold spores, *Cryptococcus neoformans,* measles virus, norovirus, influenza virus, respiratory syncytial virus (RSV), and adenovirus (Oliveira *et al.,* 2021).

Conventional methods of detecting airborne microorganisms, such as polymerase chain reaction (PCR) assays and culture-based approaches, have limitations such as high costs, lengthy procedures, and the requirement for specialized expertise and equipment (Hameed *et al.,* 2018). In response, biosensor technology, particularly aptamer-based biosensors, has emerged as a promising alternative for rapid pathogen detection. Due to its aptamers, also known as "chemical antibodies," are single-stranded DNA or RNA molecules with high specificity and affinity for target molecules (Alves Ferreira-Bravo, 2021). Aptamer-based sensing enables rapid and point-of-care examination of airborne microbes, positioning it as a frontline technology in pathogen detection (Vishwakarma *et al.,* 2021). Still aptamer presents challenges in integrating them into detection systems. By combining these aptamer into biosensor, with transducers, it can have the capability to target binding into measurable signals, enabling it as a real-time, on-site detection of airborne pathogens.

These molecules can be customized to bind specifically to a wide range of targets, including proteins, toxins, viruses, and microbial cells (Kong and Byun, 2007). The development of aptamers involve *in vitro* systematic evolution of ligands by exponential enrichment (SELEX) technique, which selects high-affinity sequences for target microorganisms. However, this process can be laborious and time-consuming (Stoltenburg *et al.,* 2013). Advances in bioinformatics have facilitated *in silico* aptamer identification, significantly reducing the time and resources needed for candidate selection. By harnessing computational biology, researchers can accelerate the discovery of aptamers tailored to detect a diverse array of airborne microbes (Alfinito *et al.,* 2023). Aptamer sequences can be optimized for improved binding affinity and specificity by using computational techniques like molecular docking and molecular dynamics simulations to predict the binding interactions between the intended aptamers and the target molecule (Cataldo *et al.,* 2018). Using structural motifs and functional groups that are known to interact with the target molecule, aptamers are developed using a different strategy called rational design (Navien *et al.,* 2021).

In silico aptamer identification allows the prediction of binding affinities, specificities, and structural characteristics before experimental validation, expediting the design and screening process. Integrating aptamer-based biosensors with *in silico* aptamer identification shows promise for real-time surveillance of airborne microbes in indoor environments. The present study was aimed to explore the potential of *in silico* techniques in designing aptamers and predicting binding diverse microbial cells found in air, with an assumption that these aptamers may facilitate the development of a sensitive detection system for real-time monitoring of airborne microbial contamination.

MATERIALS AND METHODS

The process was devised by utilizing freely accessible bioinformatics tools to forecast the tertiary configuration of RNA aptamers by starting from their sequences, and to generate docking models,

along with the identification of the residues involved in interactions with target molecule. It included four stages. The process was initiated by predicting (2D) secondary structure of aptamer from its sequence, followed by (3D) tertiary structure forecasting and integrating the secondary structure with them. Further, the molecular docking studies were used to reveal the binding affinities and molecular interactions between aptamer and its binding partner structure.

RNA aptamer identification

Sequence identification: The RNA aptamer sequences were constructed using random sequence generator tool (Piva and Giovanni, 2006). The constructed RNA aptamer sequence was analyzed using Generic Biotech oligo app [*https://www.generi-biotech.com/oligoapp/*]. The RNA sequence has been submitted NCBI Genbank database. The basic characteristic properties such as sequence length, base pair count, percentage of AC & GC content, molecular weight, optical density (1 µ mol) and temperature (°C) was retrieved. The DNA sequence were selected based upon AT/GC content and used to develop RNA aptamer.

RNA aptamer secondary structure prediction: Free energy analysis and nucleic acid sequence configuration analysis are the two primary categories of secondary structure prediction methods. Both DNA and RNA aptamers can be predicted using this computer-based prediction technique. RNA fold uses the minimum free energy concept to predict the secondary structure based on a given nucleic acid sequence. The primary RNA aptamer sequence were used to construct secondary (2D) structure of RNA aptamer. The RNAfold web server {*http://rna.tbi.univie.ac.at/***]** was used to predict secondary structures of single-stranded RNA or DNA sequences. It incorporates chemical modification constraints into a dynamic programming algorithm for the prediction of RNA secondary structure. The RNA sequence were given as input. Then the structural constraints, fold algorithm, energy parameters and output options were given and the sequence were submitted to get secondary structure.

RNA aptamer tertiary structure prediction: Accurate modelling of tertiary structure is crucial as it determines the function of a biological molecule. RNA composer [*https://rnacomposer.cs.put.poznan.pl/*] is a 3D RNA structure prediction tool that utilizes fragment analysis. This system provides a novel and easy-to-use method for predicting complex RNA 3D structures automatically. In RNA Composer, the secondary structure input is fragmented and subsequently aligned with components of the tertiary structure (Lee *et al.,* 2023). The centroid secondary structure, represented in dot-bracket notation, serves as the input, and the RNA composer predicts the tertiary 3D structure based on an iterative mode. The 3D structure model was composed and it can be stored as .pdb file.

Refining tertiary structure of RNA aptamer: The structures were loaded into BIOVIA Discovery Studio Visualizer, the software that employs algorithms to predict and add missing hydrogen atoms based on known chemical properties and bonding patterns of the atoms in molecule. These algorithms typically follow the established rules, such as bond lengths, angles, and steric hindrance. Adding hydrogen atoms is an essential step to ensure that the structural models are chemically realistic and suitable for computational analyses. It helps to improve the accuracy of calculations involving the structures and ensures that they behave appropriately in simulations and other computational studies.

Target identification

Target selection: Protein Data Bank (PDB) serves as a repository for comprehensive data pertaining to the tridimensional structural configuration of significant biological macromolecules, notably proteins and nucleic acids. This valuable resource is cultivated through collaborative global efforts, with predominant contributions stemming from the experimental techniques including X-ray crystallography and nuclear magnetic resonance spectroscopy (Goodsell, 2007). Using PDB, three dimensional structure of following targets *Staphylococcus aureus, Pseudomonas aeruginosa*, *Clostridium difficile, Aspergillus niger* var. *macrosporus*, *Candida albicans*, *Cladosporium herbarum*, influenza A virus, Coronavirus, and respiratory syncytial virus were obtained and the structures stored as .pdb file.

Target optimization: Using Biovia Discovery Studio Visualizer the .pdb protein file was prepared for docking programs. A minor regularization was done to display the missing side chains, co-crystallized ligand and water molecules. In addition to correcting and removal of water molecules locations and symmetrical alignment, hydrogen molecules were also introduced (Buglak *et al.,* 2020). Moreover, water molecules and irregular residues were eliminated, only polar hydrogen was kept and Kollman charges for protein atoms were calculated using BIOVIA.

Docking studies

HDOCK is an extensive online platform specifically developed for effective protein-protein docking. It encompasses various features including homology search, template-based modelling, structure prediction, and macromolecular docking (Yan *et al.,* 2017). Additionally, it supports protein-RNA/DNA docking and provides intrinsic scoring functions. The server offers both template-based and docking-based binding models for molecular interactions, along with options for downloading and interactive visualization of the results. The input receptor and ligand was given as .pdb file format. After submitting the receptor and ligand, the results will be sent through mail. The best models were scored in an ascending order. The docked models can be downloaded in .pdb file.

Identification and visualization of interaction between RNA Aptamer and target

The top-performing docking model, characterized by its lowest docking energy score, was chosen to determined aptamer-protein interaction sing Ucsf CHIMERA (Couch *et al.,* 2006). The PLIP web server was employed to identify the residues involved in interactions between the aptamers and their respective targets based on the obtained docking model (Salentin *et al.,* 2021). Employ colour distinctions to identify RNA, protein, and ligands. Also their intermolecular interactions, such as hydrogen bonds, hydrophobic contacts, and critical residues or nucleotides at the binding interface were analyzed.

Illustrating the mechanism of interaction between RNA aptamer and target

A visual depiction of the interaction between the target molecule and the RNA aptamer was generated using Cell Designer (Dhasmana *et al.,* 2020). Initially, key regions were identified on both the target and RNA aptamers. The potential interactions between RNA aptamer and target molecules were illustrated through directional arrows.

RESULTS AND DISCUSSION

RNA aptamers represent a hopeful approach for precisely identifying and addressing indoor air microorganisms, offering a viable means to enhance indoor air conditions and protect human well-being. The results obtained from the computational procedure presents a systematic approach to identify and characterize RNA aptamer-target interactions.

RNA aptamer identification

Sequence identification: A total of 25 sequence were generated through random sequence generator tool, from the results five best aptamers were chosen for characteristic analysis through oligo app and after analysing three best aptamers were chosen based upon their properties. The Table 2 indicates the various properties of the identified aptamers, that include sequence length, nucleotide content, composition, molecular weight and oligonucleotide extinction coefficient. RNA aptamer sequence-1 spanned 76 nucleotides with significant 68.4% AU content and a 31.6% GC content. This indicated the preference for AU-rich regions commonly observed in RNA aptamers. Its molecular weight (MW) was 22,679.1 daltons, and its oligonucleotide extinction coefficient stood at 825.7. Conversely, RNA aptamer sequence-2, comprised of 52 nucleotides, showing a slightly higher 57.7% GC content as compared to 42.3% for AU content. These suggest a preference for GC-rich regions. This sequence possessed molecular weight of 15,718.9 Da and their oligonucleotide extinction coefficient stood at

539.9. RNA aptamer sequence 3, consisting of 72 nucleotides, exhibited higher GC content (65.3%) and lower AU content (34.7%). These GC rich regions align with the most common characteristics seen among many RNA molecules. Its molecular weight was 22,044 Da, with an oligonucleotide extinction coefficient of 770.1. Specifically, none of the sequences contained inosine (I), which is an indicative of the absence of modified bases within the sequences, this could ensure essential experimental analysis.

Table 1: Characteristic properties of RNA aptamers - 1, 2 and 3

Sequences	Basic characteristics							
Sequence - 1	5'CACAUGUUGUAUCAUAUCAUUUAUGGCCGUUUUUCUUGUUGCUCGACCUAUCUUAUUCCUUUAUACCUAAAUAUAU 3'							
	Length	Count	AT/U (%)	GC (%)	I (%)	MW	OD (1 µ mol)	Tm (°C)
	76	1	68.4	31.6	0	22679.1	825.7	N/A
Sequence - 2	5'UAUCUUCGGGCGUUCUCGGCUCUGACUAUACGGUCGACAGUUUCGAGGCCC3'							
	Length	Count	AT/U (%)	GC (%)	I (%)	MW	OD (1 µ mol)	Tm (°C)
	52	1	42.3	57.7	0	15718.9	539.9	N/A
Sequence - 3	5'UCGGCUCUGAACGAACGCAGAUGGCGGUACCGGUGCCGGUUAGACGUGGAGCCGCCCUGACUACCACUGCCG3'							
	Length	Count	AT/U (%)	GC (%)	I (%)	MW	OD (1 µ mol)	Tm (°C)
	72	1	34.7	65.3	0	22044.0	770.1	N/A

Prediction of aptamer secondary and tertiary structure

The minimum free energy of secondary structure in dot bracket notation was -160, -15.2 and -23.07 kcal mol^{-1} which was reached in RNA fold. Using a RNA sequence, a study produced nucleic acid mimic (NAM) and reported the best minimal free energy within the range of -5 to -50 kcal mol^{-1} (Oliveira *et al.*, 2022). The RNA aptamer sequence 1, 2, and 3 were used to predict 3D structure. The 2D structure contained A, U, G, and C base pairs and represent them in different colours to vary their interactions, motifs, and the unpaired bases were provided with structural elements such as hairpin loops, bulges, or internal loops (Fig. 1). The specifications made us to understand the structural properties. The dot bracket notation obtained from RNA fold server was subsequently used to construct 3D structure of RNA aptamers (Fig. 2) and the folded structures with labelled residues were processed for docking.

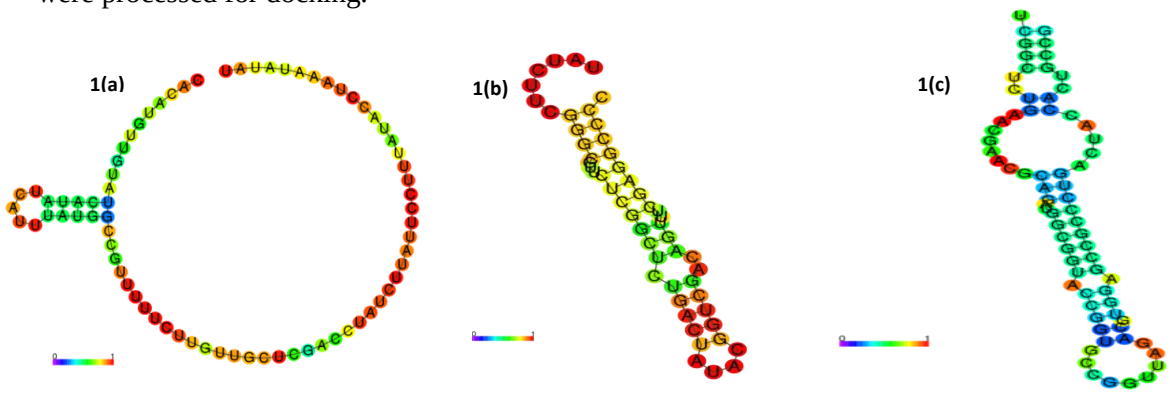

Fig. 1: Secondary structure of RNA aptamer: In Fig. 1(a), 1(b), and 1(c), the letters A, U, G and C represent RNA bases (adenine, uracil, guanine and cytosine). The lines connecting the letters represent hydrogen bonds between complementary bases (A-U and G-C). The lines form helices or stems where multiple bases are paired together are typically represented by long, continuous lines in 2D structure. The unpaired bases form loops or single-stranded regions. Different structural elements like hairpin loops, bulges, or internal loops observed within the structure. the colour given to the nucleotide bases were due to positional entropy to quantify the diversity or variability of nucleotide at specific positions within a sequence alignment.

Sequence
5'CACAUGUUGUAUCAUAUCAUUUAUGGCCGUUUUUCUUGUUGCUCGACCUAUCUUAUUCCUUUAUACCUAAAUAUAU3'
Input
5'.....(((((.....))))).....3'
Output
2(a)

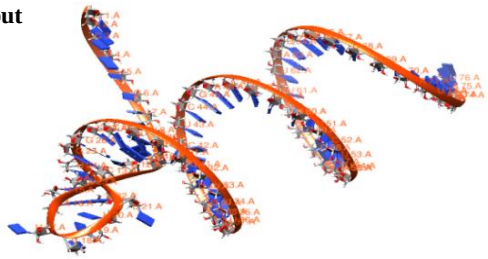

Sequence
5'UAUCUUCGGGCGUUCUCGGCUCUGACUAUACGGUCGACAGUUUCGAGGCCCC3'
Input
5' .....((((...(((((((.(((((....)))))..)))..)))))))). 3'
Output
2(b)

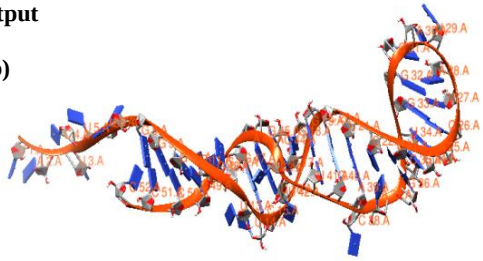

Sequence
5'UCGGCUCUGAACGAACGCAGAUGGCGGUACCGGUGCCGGUUAGACGUGGAGCCGCCCUGACUACCACUGCCG3'
Input
5'.((((..((.....(((..(((((((.(((((.....)).))))..)))))))).....))..))))3'
Output
2(c)

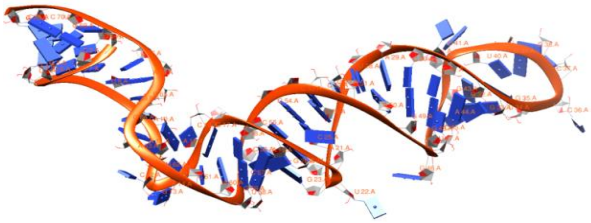

Fig. 2: Tertiary structure of RNA aptamer. Fig. 2(a), 2(b) and 2(c) represent D structure of RNA aptamer predicted through RNA Composer and refined by using BIOVIA Discovery Studio Visualizer. This involved adding the missing H-atoms and optimizing the structure for computational analysis. The refinement ensures that the structural model is chemically realistic and suitable for further studies.

Target identification

Using PDB, three dimensional structure of 9 target proteins were obtained and the structural information of proteins is shown in Table 2. Clumping factor A from *S. aureus* 1N67, *C. difficile* toxin A (TcdA) 4R04, peptidoglycan binding domain of OprF (PA1777) 5U1H (*P. aeruginosa*),

Table 2: Structural information of selected airborne pathogen associated proteins

Microbial targets	PDB ID	Resolution (Å)	Method of curation	Mutation
Clumping actor A from *Staphylococcus aureus*	IN67	2.3	XRD	Wild-type
Clostridium difficile toxin A (TcdA)	4R04	2.5	XRD	Wild-type
Peptidoglycan binding domain of OprF (PA1777) from *Pseudomonas aeruginosa*	5U1H	1.9	XRD	Wild-type
Aspergilloglutamic peptidase from *Aspergillus niger* var. *macrosporus*	1Y43	2.1	XRD	Wild-type
Als9-2 (Pt derivative) from *Candida albicans*	2Y7M	2.6	XRD	Pt- derivative mutation
Crystal structure of aldehyde dehydrogenase (ChALDH) from *Cladosporium herbarum*	7KQV	2.2	XRD	Wild-type
SARS-CoV-2 S RBD in complex with pT1611 scFV 2 from Coronavirus	8BG4	3.2	XRD	Wild-type
Non-structural protein 1 (NS1) 5VJ2 from Respiratory syncytial virus	5VJ2	2.8	Cryo-EM	Wild-type
H2 human Singapore hemagglutinin with avian receptor from influenza *A* virus	2WRB	2.7	XRD	Wild-type

PDB = Protein Data Bank; XRD = X-ray diffraction

aspergilloglutamic peptidase 1Y43 (*A. niger* var. *macrosporus*), als9-2 (Pt derivative) 2Y7M (*C. albicans*), crystal structure of aldehyde dehydrogenase (ChALDH) 7KQV (*C. herbarum*), *SARS-CoV-2* S RBD in complex with pT1611 scFV 2 8BG4 (Coronavirus), non-structural protein 1 (NS1), 5VJ2 (Respiratory Syncytial virus), H2 human singapore hemagglutinin with avian receptor 2WRB (influenza *A* virus*)* were obtained. The structures were stored as .pdb file.

Molecular docking studies

Molecular docking, evolved as a valuable computational tool, was used to explore the interaction between RNA aptamers and microbial targets. This facilitated the computational designing and optimization of aptamer based biosensor. A total of 27 docking were performed for each 3-aptamers. It showed promising binding affinity with all the 9 targets (Table 3). The obtained docking score showed

Table 3: Docking scores of RNA aptamer 1, 2, and 3 with microbial target proteins

RNA aptamer	Microbial targets	Docking score	Confidence score	Ligand RMSD (Å)
1.RNA starting with C (composite ligand, containing cytidine monophosphate)	Clumping Factor A from *Staphylococcus aureus* 1N67	-310.78	0.9614	82.72
	Clostridium difficile toxin A (TcdA) 4R04	-319.21	0.9672	453.6
	Peptidoglycan binding domain of OprF (PA1777) 5U1H (*Pseudomonas aeruginosa*)	-285.25	0.9373	57.21
	Aspergilloglutamic peptidase 1Y43 (*Aspergillus niger var. macrosporus*)	-303.29	0.9555	62.54
	Als9-2 (Pt derivative) 2Y7M *(Candida albicans)*	-299.4	0.952	105.29
	Crystal structure of aldehyde dehydrogenase (ChALDH) 7KQV *(Cladosporium herbarum)*	-344.95	0.9801	93.71
	SARS-CoV-2 S RBD in complex with pT1611 scFV 2 8BG4 (Coronavirus)	-377.13	0.9895	121.51
	Non-structural protein 1 (NS1) 5VJ2 (Respiratory syncytial virus*)*	-280.01	0.9309	68.84
	H2 human Singapore hemagglutinin with avian receptor 2WRB *(*influenza A virus)	-307.73	0.9591	98.38
2. RNA starting with U (composite ligand, containing uridine monophosphate)	Clumping Factor A from *Staphylococcus aureus* 1N67	-295.95	0.9488	101.61
	Clostridium difficile toxin A (TcdA) 4R04	-331.99	0.9672	404.84
	Peptidoglycan binding domain of OprF (PA1777) 5U1H (*Pseudomonas Aeruginosa*)	-314.48	0.9641	47.49
	Aspergilloglutamic peptidase 1Y43(*Aspergillus niger* var. *macrosporus)*	-300.16	0.9527	54.27
	Als9-2 (Pt derivative) 2Y7M (*Candida albicans*)	-297.34	0.9501	121.18
	Crystal structure of aldehyde dehydrogenase (ChALDH) 7KQV(*Cladosporium herbarum*)	-345.17	0.9802	148.65
	SARS-CoV-2 S RBD in complex with pT1611 scFV 2 8BG4 (Coronavirus)	-332.76	0.9748	100.72
	Non-structural protein 1 (NS1) 5VJ2 (Respiratory syncytial virus)	-269.99	0.9694	89.87
	H2 human Singapore hemagglutinin with avian receptor 2WRB (influenza *A* virus)	-322.71	0.9694	89.87
3. RNA starting with U (composite ligand, containing uridine monophosphate)	Clumping Factor A from *Staphylococcus aureus* 1N67	-335.27	0.979	103.88
	Clostridium difficile toxin A (TcdA) 4R04	-404.31	0.9939	379.53
	Peptidoglycan binding domain of OprF (PA1777) 5U1H (*Pseudomonas aeruginosa*)	-348.71	0.9816	73.71
	Aspergilloglutamic peptidase 1Y43(*Aspergillus niger* var. *macrosporus*)	-288.14	0.9406	68.74
	Als9-2 (Pt derivative) 2Y7M (*Candida albicans*)	-310.62	0.9613	83.6
	Crystal structure of aldehyde dehydrogenase (ChALDH) 7KQV (*Cladosporium herbarum*)	-328.44	0.9726	83.1
	SARS-CoV-2 S RBD in complex with pT1611 scFV 2 8BG4 (Coronavirus)	-395.58	0.9927	104
	Non-structural protein 1 (NS1) 5VJ2 (Respiratory syncytial virus)	-279.87	0.9307	125.54
	H2 human Singapore hemagglutinin with avian receptor 2WRB (influenza A virus)	-349.46	0.9818	95.31

the strength of binding between aptamer and its target, while higher negative scores indicated stronger interactions. Additionally, the confidence score provided an assessment of docking predictions reliability. For RNA aptamer 1, prominent docking scores were observed across all the microbial targets. This indicated the favourable binding affinities. Specifically, the interaction with crystal structure of aldehyde dehydrogenase (ChALDH) 7KQV (*C. herbarum*) and SARS-CoV-2 S RBD in complex with pT1611 scFV 2 8BG4 (Coronavirus), the docking score of -344.95 and -377.13 suggested a strong interaction. RNA aptamer 2 showed favourable docking scores with all microbial targets. This indicated robust binding interactions. Notable interactions were seen with *C. difficile* toxin A (TcdA) 4R04 and crystal structure of aldehyde dehydrogenase (*C. difficile)*, both exhibiting a docking score of -331.99 and -345.17. These scores suggested a strong binding affinity. Similarly, RNA aptamer 3 displayed strong docking scores with all microbial targets. This implied their favourable binding interactions. Notable interactions included the interaction with SARS-CoV-2 S RBD in complex with pT1611 scFV 2 8BG4 (Coronavirus) and *C. difficile* toxin A (TcdA) 4R04 (*C. difficile*), exhibiting a docking score of -395.58 and -404.31. These scores suggested a robust binding affinity. The differences in ligand RMSD values indicated variations in their structural alignment between RNA aptamer 1,2, & 3 and microbial targets.

Molecular interaction studies

The molecular interaction such as hydrogen bonds (H-bond), hydrophobic interactions, π-cation and stacking interactions, and salt bridges were studied to understand the binding affinities and interaction properties between RNA aptamers and different microbial targets e.g. surface proteins/toxins (Almazar *et al.*, 2023). The study provided a clear view on molecular recognition processes taking place at the interface between RNA aptamers and their corresponding targets (Table 4). In this study, RNA aptamer 1 showed notable interactions across multi-microbial targets. In clumping Factor A from *S. aureus* 1N67 significant hydrophobic interactions were detected with residues Val490A (3.58Å) and Lys434A (3.78Å). In addition, salt bridge interactions with Arg395A (5.37 Å) were noted. In *C. difficile* toxin A (TcdA) 4R04, the interactions were primarily phosphate-mediated, with notable interactions involving Lys1606A and Arg1651A. Similarly, in 5U1H (*P. aeruginosa*) peptidoglycan binding domain of OprF (PA1777), hydrophobic interactions with residues Ile850A and Arg1683A were

Table 4: Molecular interaction profile of RNA aptamer 1,2, and 3 with microbial target proteins

RNA aptamer	Most interacting amino acid residues	Nucleotide involved in interaction	Hydrogen bonds	Salt bridges
1. RNA starting with C (composite ligand, containing cytidine monophosphate)	Lys, Arg, Glu	Guanidine	Notable H-bond with a shortest distance of 2.27 to 3.01	Between guanidine with Lys
2. RNA starting with U (composite ligand, containing uridine monophosphate)	Lys, Arg, Glu	Guanidine, phosphate	Notable H-bond with a shortest distance of 2.40 to 2.98	Between guanidine, phosphate with Lys and Arg
3. RNA starting with U (composite ligand, containing uridine monophosphate)	Lys, Arg, Glu	Phosphate bonded guanidine	Notable H-bond with a shortest distance of 2.55 to 3.45	Between guanidine phosphate with Lys, Arg and Thy

observed, along with phosphate-mediated interactions with Lys20D and Arg65C. RNA aptamer 2 exhibited distinct interaction patterns with microbial targets. In 1N67 (*S. aureus*) clumping Factor A, significant hydrophobic interactions were noted with Val490A (3.58Å) and Lys434A (3.78Å). In 4R04 (*C. difficile)* toxin A (TcdA), interactions were primarily phosphate-mediated, with notable interactions involving Lys1687A and Asp1624A. Peptidoglycan binding domain of OprF (PA1777) 5U1H (*P. aruginosa*) showed phosphate-mediated interactions with Lys20C and Arg71D. Aspergillo-

glutamic peptidase 1Y43 (*A. niger* var. *macrosporus*) exhibited guanidine-mediated interactions with Tyr48B and Glu43B. Similarly, RNA aptamer 3 displayed unique interaction profiles. Notable interactions were observed in clumping Factor A from *S. aureus* 1N67, *C. difficile* toxin A (TcdA) 4R04 and peptidoglycan binding domain of OprF (PA1777) 5U1H (*P. aeruginosa*), with significant hydrophobic, phosphate-mediated and guanidine-mediated interactions. In Aspergilloglutamic peptidase 1Y43, interactions were primarily guanidine-mediated, while in Als9-2 (Pt derivative) 2Y7M (*C. albicans*), interactions involved phosphate bridges (Table 5). By using the above interaction study the mechanism was illustrated using cell designer (Fig. 3).

Table 5: Optimal molecular interactions between RNA aptamer 1, 2, and 3 with microbial targets

RNA aptamer	Microbial target	Optimal hydrophobic interaction (distance)	Optimal Π-cation & stacking interaction (distance)	Optimal salt bridge (distance)	Optimal hydrogen bond (distance)
RNA aptamer-1	Aspergilloglutamic peptidase 1Y43 *(Aspergillus niger* var. *macrosporus)*	Tyr45B (2.27)	Tyr45B (4.54)	Glu97B (4.37) with guanidine	Thr18A (1.98)
	Clumping Factor A from *Staphylococcus aureus* 1N67	Val490A (3.58)	Lys434A (3.78)	Arg395A (5.37) with phosphate	Asn451A (1.96)
RNA aptamer-2	Crystal structure of aldehyde dehydrogenase (ChALDH): 7KQV (*Cladosporium herbarum*)	Lys413C (5.61)	Lys413C (5.61)	Lys392A (3.54) with phosphate	-
	Peptidoglycan binding domain of OprF (PA1777) 5U1H *(Pseudomonas aeruginosa)*	-	Arg71C (1.54)	Lys20C (2.60) with phosphate	Arg71D (4.13)
RNA aptamer-3	*Clostridium difficile* toxin A (TcdA) 4R04	-	Lys1687A (5.22)	Asp1624A (5.11) with phosphate & guanidine base	His1576A (4.66)
	Non-structural protein 1 (NS1) 5VJ2 *(*Respiratory syncytial virus*)*	-	-	Lys33B (2.89) with phosphate & guanidine base	Asn70B (1.76)

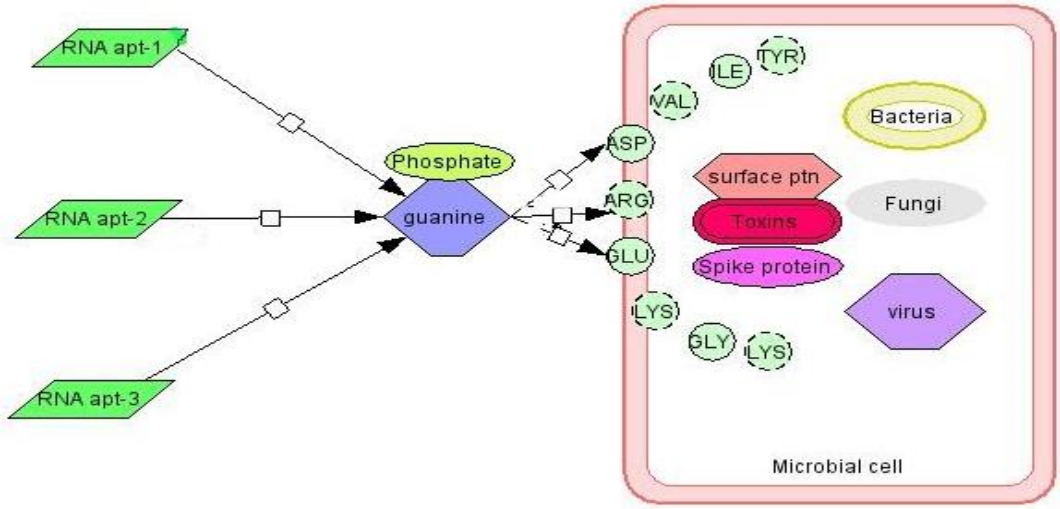

Fig. 3: Construction of mechanistic interaction model of RNA aptamer with target protein's using cell designer. This model shows mechanistics insights about the interaction of RNA aptamer 1, 2, 3 with the desired target protein like surface protein in bacteria, toxins in fungi and spike protein in virus. In this RNA aptamer 1, 2, 3 has shown promising interaction with the amino acids (Lys, Gly, Val, Asp, Arg, Aspn, Ile, Tyr) of protein through their guanidine phosphate backbone

Conclusion: The computational approaches provide here has proven valuable insights into RNA-aptamer protein interactions. It provides a robust foundation for the RNA based technologies. Through sequence analysis, secondary and tertiary prediction and docking studies we have gained a deep understanding of the molecular mechanism governing aptamer- target recognition. These insights offer various applications including real time monitoring of microbial contamination in air systems. Looking ahead, further *in-silico* studies such as molecular dynamic simulation (MDS), Computational fluid dynamics (CFD) can be done to address this gap by predicting how aptamer and target binding might alter protein folding, surface exposure of epitopes or binding pocket accessibility. Moreover, ***in****-vitro* validation technique such as and oligonucleotide synthesis can be performed to optimize the aptamers further for real time applications. Another key concept to be considered is that the epitope exchange in microbial surfaces due to genetic variation. This also presents a challenge in aptamer design, as binding sites may evolve across pathogen strains, more model with evolved possess needed to be incorporate in the sensing system for precise detection and surveillance.

Conflict of interest: The authors have no conflicts of interest regarding this investigation**.**

Acknowledgments: The authors gratefully acknowledge the Department of Science and Technology, Government of India, for providing financial support through the funds for Improvement of S&T Infrastructure in Universities and Higher Educational Institutions (FIST) program vide Grant No. SR/FIST/College-/2020/943.

REFERENCES

Acharya, B.P., Daniel, R.A., Baridalyne, N. and Gupta, S.K. 2018. Public health emergencies in urban India. *Indian Journal of Community Health*, **30**(1): 18-23.

Alfinito, E., Cataldo, R. and Millithaler, J. 2023. *In silico* studies of macromolecules as sensors. *In silico Approaches to Macromolecular Chemistry*, 533-565. [*https://doi.org/10.1016/b978-0-323-90995-2.00024-2*].

Almazar, C.A., Mendoza, M.V. and Rivera, W.L. 2023. *In silico* approaches for the identification of Aptamer binding interactions to *Leptospira* spp. Cell surface proteins. *Tropical Medicine and Infectious Disease*, **8**(2): 125. [*https://doi.org/10.3390/tropicalmed8020125*].

Alves Ferreira-Bravo, I. and DeStefano, J.J. 2021. Xeno-nucleic acid (XNA) 2'-fluoro-arabino nucleic acid (FANA) aptamers to the receptor-binding domain of SARS-Cov-2 S protein block ACE2 binding. *Viruses*, **13**(10): 1983. [*https://doi.org/10.3390/v13101983*].

Annadurai, G., Joseph Mathews, A., Krishnan, E.N. and Simonson, C.J. 2024. A review of experimental methods to determine bioaerosol transfer in energy recovery ventilators. *Applied Thermal Engineering*, **240**: 122322. [*https://doi.org/10.1016/j.applthermaleng.2023.122322*].

Buglak, A.A., Samokhvalov, A.V., Zherdev, A.V. and Dzantiev, B.B. 2020. Methods and applications of *in silico* aptamer design and modeling. *International Journal of Molecular Sciences*, **21**(22): 8420. [*https://doi.org/10.3390/ijms21228420*].

Cataldo, R., Ciriaco, F. and Alfinito, E. 2018. A validation strategy for *in silico* generated aptamers. *Computational Biology and Chemistry*, **77**: 123-130.

Chawla, H., Anand, P., Garg, K., Bhagat, N., Varmani, S.G., Bansal, T., *et al.*, 2023. A comprehensive review of microbial contamination in the indoor environment: Sources, sampling, health risks, and mitigation strategies. *Frontiers in Public Health*, **11**: [*https://doi.org/10.3389/fpubh.2023.1285393*].

Couch, G.S., Hendrix, D.K. and Ferrin, T.E. 2006. Nucleic acid visualization with UCSF chimera. *Nucleic Acids Research*, **34**(4): e29. [*https://doi:10.1093/nar/gnj031*].

Dhasmana, A., Uniyal, S., Anukriti, Kashyap, V.K., Somvanshi, P., Gupta, M., Bhardwaj, U., *et al.*, 2020. Topological and system-level protein interaction network (PIN) analyses to deduce molecular mechanism of curcumin. *Scientific Reports*, **10**(1): [*https://doi.org/10.1038/s41598-020-69011-0*].

Gonzalez-Martin, C. 2019. *Airborne Infectious Microorganisms. Encyclopedia of Microbiology*, **2019**: 52-60. [*https://doi.org 10.1016/B978-0-12-809633-8.13002-X*].

Goodsell, D. 2011. *PDB Pioneers*. RCSB Protein Data Bank. [*https://doi:10.2210/rcsb_pdb/mom_2011_10*].

Hameed, S., Xie, L. and Ying, Y. 2018. Conventional and emerging detection techniques for pathogenic bacteria in food science: A review. *Trends in Food Science & Technology*, **81**: 61-73.

Kong, H.Y. and Byun, J. 2013. Nucleic acid aptamers: New methods for selection, stabilization, and application in biomedical science. *Biomolecules and Therapeutics*, **21**(6): 423-434.

Lee, S.J., Cho, J., Lee, B., Hwang, D. and Park, J. 2023. Design and prediction of aptamers assisted by *in silico* methods. *Biomedicines*, **11**(2): 356. [*https://doi.org/10.3390/biomedicines11020356*].

Morawska, L. and Huang, W. 2022. WHO health guidelines for indoor air quality and national recommendations/Standards. *Handbook of Indoor Air Quality*, 1-20. [*https://doi.org/10.1007/978-981-10-5155-5_49-1*].

Navien, T.N., Thevendran, R., Hamdani, H.Y., Tang, T. and Citartan, M. 2021. *In silico* molecular docking in DNA aptamer development. *Biochimie*, **180**: 54-67.

Oliveira, R., Pinho, E., Sousa, A.L., DeStefano, J.J., Azevedo, N.F. and Almeida, C. 2022. Improving aptamer performance with nucleic acid mimics: De Novo and post-SELEX approaches. *Trends in Biotechnology*, **40**(5): 549-563.

Oliveira, R., Pinho, E., Sousa, A.L., DeStefano, J.J., Azevedo, N.F. and Almeida, C. 2022. Modelling aptamers with nucleic acid mimics (NAM): From sequence to three-dimensional docking. *PLOS ONE*, ***17*(**3), e0264701.[*https://doi.org1371/journal.pone.0264701*].

Piva, F. and Giovanni, P. 2006. RANDNA: A random DNA sequence generator. *In Silico Biology*, **6**(3): 253-258.

Salentin, S., Schreiber, S., Haupt, V.J., Adasme, M.F., Schroeder, M. 2015. PLIP: Fully automated protein-ligand interaction profiler. *Nucleic Acids Research*, **43**(W1): W443-W447.

Stoltenburg, R., Reinemann, C. and Strehlitz, B. 2007. SELEX - A (r) evolutionary method to generate high-affinity nucleic acid ligands. *Biomolecular Engineering*, **24**(4): 381-403.

Vishwakarma, A., Lal, R. and Ramya, M. 2021. Aptamer-based approaches for the detection of waterborne pathogens. *International Microbiology*, **24**(2): 125-140.

Yan, Y., Zhang, D., Zhou, P., Li, B. and Huang, S. 2017. HDOCK: A web server for protein–protein and protein–DNA/RNA docking based on a hybrid strategy. *Nucleic Acids Research*, **45**(W1): W365-W373.